ATR-FTIR spectroscopic studies on density changes of fused silica induced by localized CO_2 laser treatment

Zhang Chuan-Chao(张传超)[a], Zhang Li-Juan(张丽娟)[a], Liao Wei(廖 威)[a], Yan Zhong-Hua(晏中华)[b], Chen Jing(陈 静)[a]†, Jiang Yi-Lan(蒋一岚)[a], Wang Hai-Jun(王海军)[a], Luan Xiao-Yu(栾晓雨)[a], Ye Ya-Yun(叶亚云)[a]‡, Zheng Wan-Guo(郑万国)[a], and Yuan Xiao-Dong(袁晓东)[a]

[a] *Research Center of Laser Fusion, China Academy of Engineering Physics, Mianyang* 621900, *China*
[b] *School of Physical Electronics, University of Electronic Science and Technology of China, Chengdu* 610054, *China*

(Received 15 July 2014; revised manuscript received 12 September 2014; published online 10 December 2014)

The surface density changes of the central region of the sites treated by using the CO_2 laser-based non-evaporative damage mitigation for fused silica are investigated by attenuated total reflectance-Fourier transform infrared spectroscopy (ATR-FTIR). The ATR-FTIR peak shifts of the treated sites of fused silica are monitored to determine the changes of the corresponding density. For the quenching treated sites, the surface density is increased by (0.24±0.01)% compared with the initial density but the laser annealing by the exposure of a power ramp down after damage mitigation effectively suppresses the structural changes of treated sites, which could reduce the increase of the corresponding density to (0.08±0.01)%. The results provide sufficient evidence that the laser annealing by a power ramp down after damage mitigation has a positive effect on the control of the structural change induced by CO_2 laser-based damage mitigation.

Keywords: fused silica, damage mitigation, ATR-FTIR, laser annealing

PACS: 42.70.Ce, 61.80.–x, 63.50.–x, 78.20.–e **DOI:** 10.1088/1674-1056/24/2/024220

1. Introduction

Fused silica is universally used to make large aperture optics, such as windows, lenses, gratings, and debris shields, in high-power UV laser systems. One of the major concerns encountered for these high-cost fused silica optics is laser-induced surface damage under the exposure of high-fluence UV laser.[1–6] For the high-power UV laser facilities, such as the National Ignition Facility (NIF) in USA,[7] the Laser Mega Joule in France,[8] and the SGIII laser facility in China,[9,10] the routine operation is above the damage growth threshold of fused silica optics. Once the surface damages are initiated under the high-fluence UV laser irradiation, they will grow exponentially with subsequent laser shots, and will result in excessive light scattering and beam modulation, and they will finally lead to a shortening of the lifetime of fused silica optics.[11] Surface damage of the fused silica optics intensively restricts the maximum output fluence of the high-power UV laser facilities, and abilities to mitigate the laser damage and enhance the damage growth threshold are necessary for the routine operation of these facilities.

A variety of techniques have been developed to mitigate the growth of surface damage and the most effective technique is the CO_2 laser processing technique to locally melt or evaporate the damage[12] There are two kinds of CO_2 laser mitigation protocols, i.e., evaporative protocol and no-evaporative protocol.[8,13–16] Compared with the evaporative mitigation protocol, the non-evaporative mitigation protocol has the advantage of minimal surface perturbation or material removal and it only needs a simple system setup.[8,15,16] However, some problems, such as raised rims, re-deposited debris, bubbles or residual stress at the mitigated damage sites, may occur when using the non-evaporative mitigation protocol and they will lead to problematic damage re-initiation and growth, as well as downstream intensification. Extensive investigations have been conducted to solve these problems,[4,8,15–24] and the non-evaporative mitigation protocol with the combination of particular powers and exposure times of CO_2 laser can effectively eliminate raised rims, re-deposited debris, and bubbles at the mitigated damage sites.[8,15–22] In addition, high temperature oven annealing or laser annealing can effectively control the residual stress to an acceptable level.[21–24] These modifications of the mitigated damage sites induced by intensive CO_2 laser treatment are associated with the local structural changes of fused silica. However, few studies on the structural changes of fused silica treated with localized CO_2 laser heating have been reported. Only recently have Matthews *et al.* reported their study on fused-silica microstructural changes induced by CO_2 laser treatment by using Raman microscopy.[25] Considering the fact that the properties of fused silica are strongly dependent on the structure, it is important to systematically study the structural changes of fused silica for non-evaporative mitigation.

†Corresponding author. E-mail: chenjing_19901102@163.com
‡Corresponding author. E-mail: yeyayun8617@163.com

© 2015 Chinese Physical Society and IOP Publishing Ltd

In fused silica, each silicon atom is surrounded by four tetrahedrally co-ordinated oxygen atoms, and adjacent silicon atoms are bridge-bonded through a single oxygen atom. Interatomic vibrational modes of Si–O–Si bonding strongly depend on Si–O–Si bonding angle.[26] Infrared (IR) spectroscopy has been widely used to characterize the structure of fused silica, and the correlation between the IR peak position of silica structural band and the frozen-in temperature of fused silica, i.e., fictive temperature of fused silica, has been established.[26,27] The structure of fused silica depends on the fictive temperature, and the relationship between fictive temperature and glass density has been reported.[28] Thus, the density change of fused silica induced by localized CO_2 laser treatment can be measured by the IR technique. Attenuated total reflectance-Fourier transform infrared spectroscopy (ATR-FTIR) is a powerful means for the direct surface characterization of solids. In this work, systematic investigations of the fused silica treated by the CO_2 laser non-evaporative mitigation are performed by using ATR-FTIR technique. The density change of fused silica during CO_2 laser treatment is estimated by the shift of the IR peak position of the silica structural band.

2. Experimental details

The fused silica samples used in this study are polished UV-grade Corning 7980 fused silica, 40-mm square by 4-mm thick. Before being treated by CO_2 laser, the fused silica samples were slightly etched in a buffered hydrofluoric (HF) acid solution and then cleaned by deionized water. A commercial radio frequency power excited CO_2 laser (Coherent GEM-100 L) with a maximum output power of 100 W and power stability of $\pm 3\%$ was used to treat the fused silica samples. The spatial profile of the CO_2 laser beam is a Gaussian distribution. A beam spot with a diameter of 3 mm, where the beam spot intensity decreases to $1/e$ times of its central intensity, at the sample surface was obtained by a ZnSe lens with a 200-mm focal length for the treatment of the samples. For the non-evaporative mitigation protocol, the fused silica samples were first preheated at a low laser power of 13.7 W for 30 seconds. They were next irradiated under a high power of 25.3 W for 4 seconds to heat the fused silica to above the melting point and heal the damages. Then, laser annealing by a variety of linear decreases in the CO_2 laser power with lower power heating silica below the melting point from 19.7 W to 8.7 W with different exposure times was performed to minimize the structural changes of the irradiated sites on the surface of the fused silica sample.

The treated sites of fused silica were first characterized with a photoelastic tool (PTC-702) to determinate the measurement region of the irradiated sites. The ATR-FTIR spectra were measured by a Nicolet 5700 spectrometer equipped with an ATR accessory. The measurements were carried out in a range of 700 cm^{-1}–1400 cm^{-1}, with a Ge ATR crystal, 64 scans and resolution of 1 cm^{-1}.

To calibrate the fictive temperature of the measurement region of fused silica, a thin fused silica slice with 10-mm square by 1-mm thick was treated by the CO_2 laser with a 4-mm diameter beam spot and 26.3-W power for the sufficient length of time of about 100 seconds to establish a metastable equilibrium state at the central portion of the irradiated site, and it was then air quenched. The ATR-FTIR spectra of the central portion of the irradiated site were measured, and the corresponding FTIR transmission spectra were also measured for calibration.

3. Results and discussion

Figure 1(a) shows a typical image of a site treated with the non-evaporative mitigation protocol by a photoelastic tool (PTC-702). Generally, for a typical non-evaporative mitigation protocol, the irradiated zone of the fused silica sample intensively absorbs the energy of a CO_2 laser beam, which induces a rapid temperature increase in the irradiated zone. As the fused silica in the irradiated zone is heated up to a peak temperature exceeding the glass transition temperature, the material of the damage site is melted and healed, and then a rapid thermal quench ensues following the switching-off of the CO_2 laser. The melt zone of the treated site cannot completely relax the strained material over a time that is much shorter than the corresponding structural relaxation time, and a structure corresponding to a high metastable equilibrium temperature is frozen at higher density. Consequently, the melt zone is intensively plastically deformed, which will induce the change of the morphology profile of the irradiated zone and the formation of residual stress at the treated site.

For a typical treated site, the distribution of the residual stress is shown in Fig. 1(a). If a small damage is introduced at the treated site, the residual stress may cause the cracks of the introduced damage to propagate away, as shown in Fig. 1(b), which leads to a catastrophic failure of the fused silica optics. Meanwhile, the laser annealing by a linear ramp down of the CO_2 laser power following the damage mitigation can effectively suppress the residual stress. As shown in Fig. 1(c), large damages are introduced at the treated site and the residual stress does not cause the cracks of the introduced damages to propagate away, which suggests that the local structure of the treated site must be changed during the laser annealing.

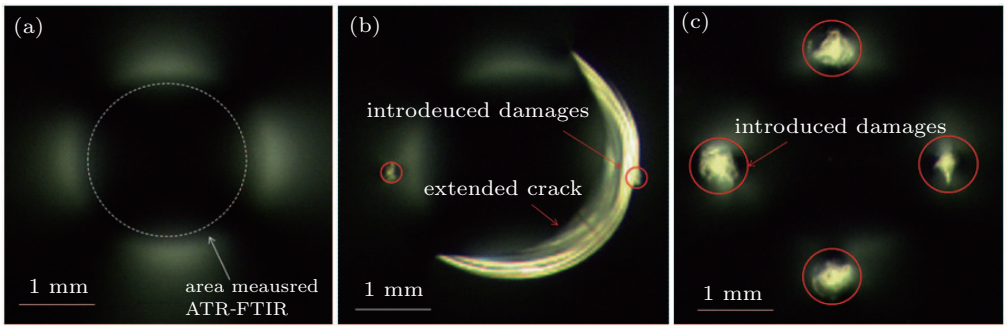


Fig. 1. (color online) (a) Typical image of a treated site observed by a photoelastic tool (PTC-702), (b) a typical image of fracture extending induced by introduced small damages for the treated site, and (c) a typical image of introduced large damages for the treated site with laser annealing following the damage mitigation, no fracture extension is observed.

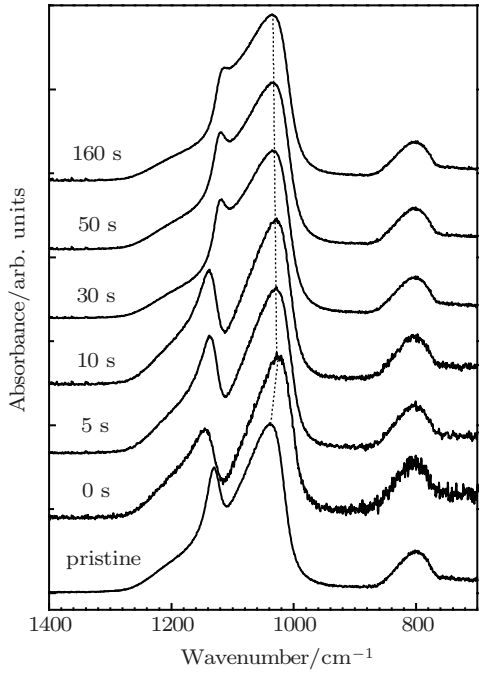


Fig. 2. ATR-FTIR spectra in various exposure times of the laser annealing by the linear power ramp down after the damage mitigation.

To precisely determine the structural changes of the treated sites, the central region of the irradiated site, as shown in Fig. 1(a), is measured by the ATR-FTIR technique. The ATR-FTIR spectra with laser annealing in various exposure times of the power ramp down after the damage mitigation are shown in Fig. 2. For the pristine fused silica, three main peaks at 804.1 cm^{-1}, 1036.9 cm^{-1}, and 1130.4 cm^{-1} are observed in a range of 700 cm^{-1}–1400 cm^{-1}. According to the reported literature,[27,29] the reflection peak at 804.1 cm^{-1} is attributed to the bending vibration of Si–O–Si bridges, and the reflection peak at 1036.9 cm^{-1} is ascribed to the transverse-optic (TO) component of the asymmetric stretching vibration of Si–O–Si bridges, and the reflection peak at 1130.4 cm^{-1} arises from the longitudinal-optic (LO) component of the asymmetric stretching vibration of Si–O–Si bridges. The TO asymmetric stretching vibrational mode of Si–O–Si bridge has been widely used to determine the fictive temperature of fused silica and in the present study the shift in this main band is monitored to characterize the structural changes of the treated sites of fused silica by a CO_2 laser. As shown in Fig. 2, the TO vibrational mode with quenching after the damage mitigation has shifted to a lower wavenumber than that of the pristine sample, the peak position gradually increases with the increasing exposure time of the laser annealing by the power ramp down after the damage mitigation.

The changes of the TO asymmetric stretching vibrational mode of Si–O–Si bridges indicate the structural changes of the treated sites during the non-evaporative mitigation. The peak position of the TO vibrational mode as a function of exposure time of the laser annealing by the power ramp down after the damage mitigation is shown in Fig. 3. From the reported empirical relation between the fictive temperature and the peak position of TO vibrational mode, the fictive temperature of the mitigated sites can be directly determined by using the non-evaporative mitigation. Unfortunately, the peak position of TO vibrational mode varies with incidence angle,[29] and the incidence angle in the present ATR-FTIR study is different from the almost normal incidence angle for the reported empirical relation between fictive temperature and the peak position,[27] so we cannot directly use the reported empirical relation to estimate the corresponding fictive temperature of the treated sites. Meanwhile, it is reported that the peak position of the structural band near 2260 cm^{-1} in IR transmission spectrum, which is attributed to the overtone of the asymmetric stretching vibration of the Si–O–Si bridges, is linearly correlated with the peak position of the TO asymmetric stretching vibration of Si–O–Si bridges.[27] The peak position of IR transmission spectrum at around 2260 cm^{-1} is also widely useful for determining the fictive temperature of fused silica, and the precise relation between the peak position and the corresponding fictive temperature from 1000 °C to 1550 °C has been established as,[26]

$$\nu_{\mathrm{p}} = 2221.2 + 6.1086\left(\frac{10^4}{T_{\mathrm{f}}}\right) - 0.097385\left(\frac{10^4}{T_{\mathrm{f}}}\right)^2, \quad (1)$$

where, ν_p is the peak position of IR transmission spectrum at around 2260 cm^{-1} and T_f is the fictive temperature of fused silica.

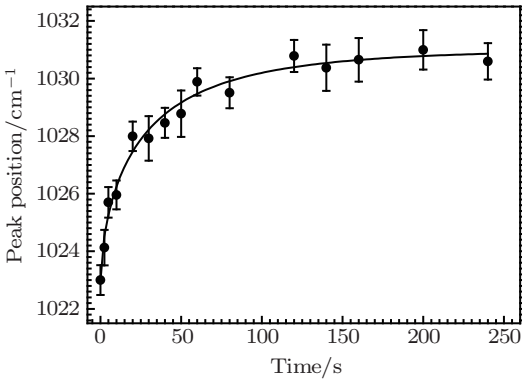


Fig. 3. Peak position of the TO asymmetric stretching vibration of Si–O–Si bridges as a function of exposure time of the laser annealing by the power ramp down after damage mitigation.

The relation between the peak position of the overtone of the asymmetric stretching vibration of Si–O–Si bridge in IR transmission spectrum and the peak position of the TO asymmetric stretching vibration of Si–O–Si bridge in ATR-FTIR spectra is calibrated by a thin fused silica slice. The thin fused silica slice is treated by CO_2 laser for a sufficient length of time to establish a metastable equilibrium state at the central portion of the irradiated zone. Figures 4(a) and 4(b) show the ATR-FTIR spectra and IR transmission spectra of the pristine sample and the treated sample, respectively. For the pristine sample, the peak position of TO asymmetric stretching vibrational mode is at 1036.9 cm^{-1} and the peak position of the overtone of the asymmetric stretching vibrational mode is at 2262.7 cm^{-1}. For the treated sample, the peak position of TO asymmetric stretching vibrational mode is at 1026.3 cm^{-1} and the peak position of the overtone of the asymmetric stretching vibrational mode is at 2253.6 cm^{-1}. According to the linear relationship,[27] the relation of the peak position of the overtone of the asymmetric stretching vibrational mode to the peak position of TO asymmetric stretching vibrational mode can be written as,

$$\nu_p = 1376.8 + 0.8544\nu_{TO}, \tag{2}$$

where, ν_{TO} is the peak position of TO asymmetric stretching vibration of Si–O–Si bridge in the ATR-FTIR spectra.

Thus, the fictive temperature of the treated site can be evaluated by the combination of Eq. (1) and Eq. (2). In addition, ν_{TO} as a function of exposure time of the laser annealing by the power ramp down after the damage mitigation, as shown in Fig. 3, can be converted into T_f as a function of exposure time of the laser annealing by the power ramp down after the damage mitigation, as shown in Fig. 5. One of the major concerns is whether the combination of Eq. (1) and Eq. (2) can correctly evaluate the fictive temperature of the treated site. For the quenching mitigated site without the exposure of the laser annealing by the power ramp down after damage mitigation, $\nu_{TO} = (1023.5 \pm 0.5)$ cm^{-1}, and from Eqs. (1) and (2), $T_f = (1880 \pm 30)$ K, which is consistent with the reported $\sim$ 1900 K for the surface of quenching mitigated sites.[24] For the pristine fused silica sample, $\nu_{TO} = (1036.9 \pm 0.5)$ cm^{-1}, and from Eqs. (1) and (2), $T_f = (1286 \pm 15)$ K, which is consistent with the annealing temperature 1315 K for the Corning 7980 fused silica. These results evidently indicate that the combination of Eq. (1) and Eq. (2) can correctly estimate the fictive temperature of the mitigated site from the TO vibrational mode ν_{TO}. Figure 5 indicates that the fictive temperature first decreases abruptly with the increase of the exposure time and then gradually changes to a steady value. With the increase of the exposure time of the laser annealing by the power ramp down, the cooling rate of the material at the treated site is slower and the structure of the material, which reaches the high equilibrium temperature, has sufficient time to gradually relax to the state corresponding to the low fictive temperature during the decrease of the thermodynamic temperature. The minimum fictive temperature is stable at (1505±28) K for the non-evaporative mitigation by the 3-mm-diameter beam spot, which indicates that the laser annealing by the power ramp down can control the mitigated sites to lower the fictive temperature.

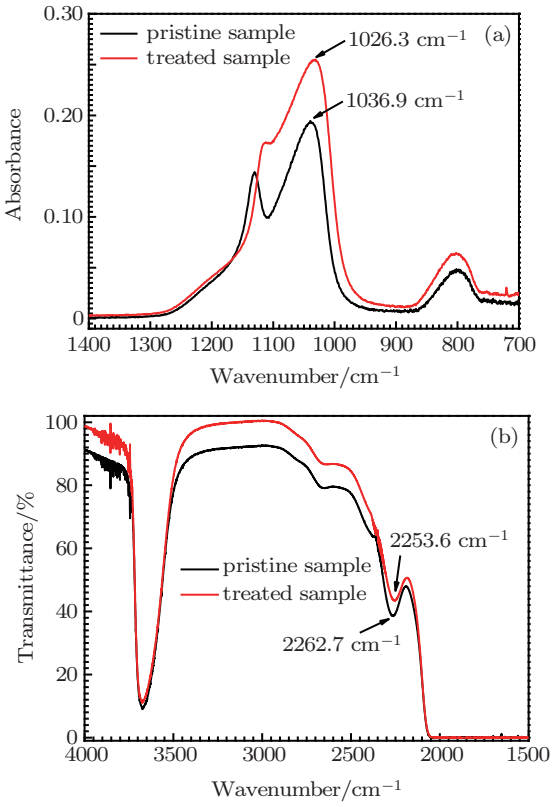


Fig. 4. (color online) ATR-FTIR spectra (a) and IR transmission spectra (b) of pristine sample and the central portion of the sample treated by 26.3-W power with a 4-mm diameter CO_2 laser spot.

The fictive temperature changes with exposure time of the laser annealing by the power ramp down after the damage mitigation have been converted into the corresponding density change. The UV-grade Corning 7980 fused silica used in this experiment belongs to the Type III silica glass.[30] For the Type III silica glass at a temperature in a range from 1000 °C to 1450 °C, the relationship between the normalized density difference and the fictive temperature of fused silica is linear and can be described as[28]

$$\Delta\rho/\rho\ \text{(ppm)} = 4.265T_{\rm f}\ (^{\circ}\text{C}) - 5370. \tag{3}$$

Since the density of the Corning 7980 fused silica at room temperature for the sample with 1042-°C fictive temperature is 2.20 g/cm^3 in this experiment, from Eq. (3), the relation between the density and the fictive temperature of the Corning 7980 fused silica can be written as

$$\rho\ (\text{g/cm}^3) = 9.39\times10^{-6}T_{\rm f}\ (^{\circ}\text{C}) + 2.1902. \tag{4}$$

Using this relation, the density near the surface of the central region of the treated site can be evaluated from the fictive temperature, and the results are shown in Fig. 5. Because the density is linear with respect to the fictive temperature, the change evolution of the density is similar to that of the fictive temperature. For the quenching treated sites without laser annealing after damage mitigation, the surface density of the central portion enhances (0.24±0.01)% compared with for the pristine sample site. The laser annealing by the power ramp down after damage mitigation effectively suppresses the density change and the minimum increase of surface density of the mitigated sites can be reduced to (0.08±0.01)% compared with that of the pristine sample site.

The experimental data of the surface density of the central region of the treated site with increasing exposure time of the laser annealing by the power ramp down are well fitted to the following equation:

$$\rho\,(t) = \rho_0 + A\times\exp(-(t/\tau)^{\beta}), \tag{5}$$

where $\rho\,(t)$ is the surface density of the central portion of the treated sites with exposure time t of the power ramp down, $\rho_0 = (2.2042\pm0.0002)$ g/cm^3 is the surface density of the central portion of the treated sites with infinite exposure time, $A = (0.0037\pm0.0002)$ g/cm^3 is a time-independent constant, $\tau = (23\pm4)$ s is the average relaxation time, and $\beta = (0.60\pm0.08)$ is the stretched exponential parameter. This density evolution of the treated sites with increasing exposure time of the laser annealing by the power ramp down is consistent with the stretched exponential Kohlrausch–William–Watts function for the structural relaxation of glass that was reported by Scherer.[31]

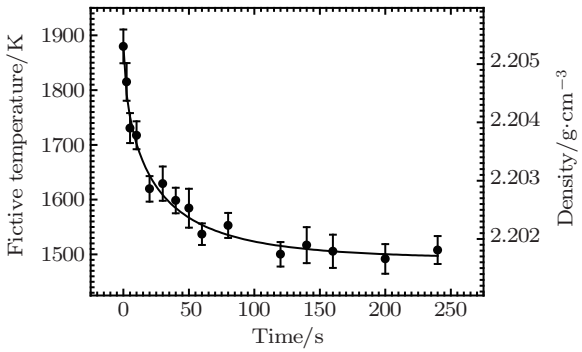


Fig. 5. Fictive temperature and average density of the central surface of the mitigated site, each as a function of exposure time of the laser annealing by the power ramp down after damage mitigation.

4. Conclusions

The surface density changes of the central portion of the sites treated by using the CO_2 laser-based non-evaporative mitigation are investigated by ATR-FTIR spectra. The ATR-FTIR peak shifts of the treated sites of fused silica are monitored to determine the changes of the fictive temperature and the corresponding density. For the quenching treated sites, the surface fictive temperature of the treated site increases up to (1880±30) K, and the corresponding density is increased by (0.24±0.01)% compared with the initial density. Laser annealing by the exposure of a power ramp down after damage mitigation effectively suppresses the structural change, which could reduce the fictive temperature of the treated sites to (1505±28) K and minimize the increase of the corresponding density to (0.08±0.01)% of the initial density. These results provide sufficient evidence that laser annealing by a power ramp down after damage mitigation has a positive effect on the control of the structural change induced by CO_2 laser-based damage mitigation.

References

[1] Campbell J H, Hawley-Fedder R A, Stolz C J, Menapace J A, Borden M R, Whitman P K, Yu J, Runkel M, Riley M O, Feit M D and Hackel R P 2004 *Proc. SPIE* **5341** 84
[2] Carr C W, Bude J D and DeMange P 2010 *Phys. Rev. B* **82** 184304
[3] Zhang C L, Li X B, Wang Z G, Liu C M, Xiang X, Lv H B, Yuan X D and Zu X T 2011 *Chin. Phys. Lett.* **28** 074205
[4] Zhang C L, Liu C M, Xiang X, Wang Z G, Li L, Yuan X D, He S B and Zu X T 2012 *Acta Phys. Sin.* **61** 164207 (in Chinese)
[5] Zhang C L, Yuan X D, Xiang X, Wang Z G, Liu C M, Li L, He S B and Zu X T 2012 *Chin. Phys. B* **21** 094213
[6] Li L, Xiang X, Yuan X D, He S B, Jiang X D, Zheng W G and Zu X T 2013 *Chin. Phys. B* **22** 054207
[7] Folta J, Nostrand M, Honig J, Wong N, Ravizza F, Geraghty P, Taranowski M, Johnson G, Larkin G, Ravizza D, Peterson J, Welday B and Wegner P 2013 *Proc. SPIE* **8885** 88850Z
[8] Palmier S, Gallais L, Commandre M, Cormont P, Courchinoux R, Lamaignere L, Rullier J L and Legros P 2009 *Appl. Surf. Sci.* **255** 5532
[9] Han W, Huang W Q, Wang F, Li K Y, Feng B, Li F Q, Jing F and Zheng W G 2010 *Chin. Phys. B* **19** 106105
[10] Han W, Wang F, Zhou L D, Feng B, Jia H T, Li K Y, Xiang Y and Zheng W G 2012 *Chin. Phys. B* **21** 077901
[11] Norton M A, Adams J J, Carr C W, Donohue E E, Feit M D, Hackel R P, Hollingsworth W G, Jarboe J A, Matthews M J, Rubenchik A M and Spaeth M L 2008 *Proc. SPIE* **6720** 67200H

[12] Hrubesh L W, Norton M A, Molander W A, Donohue E E, Maricle S M, Penetrante B M, Brusasco R M, Grundler W, Butler J A, Carr J W, Hill R M, Summers L J, Feit M D, Rubenchik A, Key M H, Wegner P J, Burnham A K, Hackel L A and Kozlowski M R 2002 *Proc. SPIE* **4679** 23
[13] Bass I L, Guss G M and Hackel R P 2005 *Proc. SPIE* **5991** 59910C
[14] Bass I L, Guss G M, Nostrand M J and Wegner P J 2010 *Proc. SPIE* **7842** 784220
[15] Adams J J, Bolourchi M, Bude J D, Guss G M, Matthews M J and Nostrand M C 2010 *Proc. SPIE* **7842** 784223
[16] Mendez E, Nowak K M, Baker H J, Villarreal F J and Hall D R 2006 *Appl. Opt.* **45** 5358
[17] Xiang X, Zheng W G, Yuan X D, Dai W, Jiang Y, Li X B, Wang H J, Lu H B and Zu X T 2011 *Chin. Phys. B* **20** 044208
[18] Li L, Xiang X, Zu X T, Yuan X D, He S B, Jiang X D and Zheng W G 2012 *Chin. Phys. B* **21** 044212
[19] Dai W, Xiang X, Jiang Y, Wang H J, Li X B, Yuan X D, Zheng W G, Lv H B and Zu X T 2011 *Opt. Laser Eng.* **49** 273
[20] Liu C M, Jiang Y, Luo C S, Shi X Y, Ren W, Xiang X, Wang H J, He S B, Yuan X D, Lv H B, Zheng W G and Zu X T 2012 *Chin. Phys. Lett.* **29** 044211
[21] Jiang Y, Liu C M, Luo C S, Yuan X D, Xiang X, Wang H J, He S B, Lu H B, Ren W, Zheng W G and Zu X T 2012 *Chin. Phys. B* **21** 054216
[22] Jiang Y, Xiang X, Liu C M, Luo C S, Wang H J, Yuan X D, He S B, Ren W, Lu H B, Zheng W G and Zu X T 2012 *Chin. Phys. B* **21** 064219
[23] Yu J X, He S B, Xiang X, Yuan X D, Zheng W G, Lu H B and Zu X T 2012 *Chin. Phys. B* **21** 064401
[24] Matthews M J, Stolken J S, Vignes R M, Norton M A, Yang S, Cooke J D, Guss G M and Adams J J 2009 *Proc. SPIE* **7504** 750410
[25] Matthews M J, Vignes R M, Cooke D, Yang S T and Stolken J S 2010 *Opt. Lett.* **35** 1311
[26] Kakiuchida H, Saito K and Ikushima A J 2003 *J. Appl. Phys.* **93** 777
[27] Agarwal A, Davis K M and Tomozawa M 1995 *J. Non-Cryst. Solids* **185** 191
[28] Shelby J E 2004 *J. Non-Cryst. Solids* **349** 331
[29] Almeida R M 1992 *Phys. Rev. B* **45** 161
[30] Numata K, Yamamoto K, Ishimoto H, Otsuka S, Kawabe K, Ando M and Tsubono K 2004 *Phys. Lett. A* **327** 263
[31] Scherer G W 1990 *J. Non-Cryst. Solids* **123** 75